Energy Engineering

Tech Science Press

https://doi.org/10.32604/ee.2026.076328

ARTICLE

Data-Driven and Physics-Informed Surrogate Modeling for Heat Conduction in the Pressurizer Wall of Pressurized Water Reactors under Severe Accident Scenarios

Fabiano Thulu and Zeyun Wu*

Department of Mechanical and Nuclear Engineering, Virginia Commonwealth University, Richmond, VA, USA

*Corresponding Author: Zeyun Wu. Email: zwu@vcu.edu

Received: 18 November 2025; Accepted: 22 January 2026

ABSTRACT: Real-time prediction of temperature distribution in the pressurizer walls of Pressurized Water Reactors (PWRs) during severe accidents, such as Station Blackout (SBO) and Loss-of-Coolant Accident (LOCA) is vital for structural integrity assessment. However, conventional thermal-hydraulic simulations used for such predictions are computationally intensive, limiting their applicability for real-time analysis. This study develops and compares three surrogate models: Polynomial Regression, Deep Neural Network (DNN), and a Physics-Informed Neural Network (PINN). Thermal-hydraulic simulation data generated by RELAP5-3D are integrated with physics-constrained learning techniques to model transient heat conduction in the pressurizer wall. The internal wall temperature evolution is reconstructed using a one-dimensional transient heat conduction mode solved via the Finite Difference Method. The Polynomial Regression model, while achieving a relative high coefficient of determination (R^2 = 0.9780), exhibited an average Root Mean Squared Error (RMSE) of 7.50 K and a Maximum Absolute Error (MaxAE) of 193.6 K on unseen test data, indicating limited capability in capturing localized thermal stresses. In contrast, the purely data-drive DNN model demonstrated superior performance, achieving an overall test R^2 of 0.9996, an RMSE of 1.04 K, and a significantly reduced MaxAE of 24.8 K. Finally, the PINN model yielded an overall physics-based test R^2 of 0.9874, with an RMSE of 5.66 K, and a MaxAE of 89.7 K. Although the DNN achieves the highest statistical accuracy, the PINN offers a key advantage by enforcing adherence to the governing heat conduction equations. The embedded physical consistency makes PINN a more reliable and trustworthy surrogate for nuclear safety analysis, where maintaining physical fidelity is as critical as numerical accuracy.

KEYWORDS: Heat conduction; surrogate modeling; polynomial regression; deep neural networks; physics-informed neural networks

1 Introduction

Pressurized Water Reactors (PWRs) have proven to be a cornerstone of global reliable and clean energy source [1]. Within a PWR, the pressurizer plays a critical role in maintaining primary coolant pressure and regulating volume changes induced by temperature fluctuations [2]. The dynamic thermal-hydraulic (T/H) behavior within the pressurizer involves complex multiphase and multiphysics phenomena, including heat transfer, phase change and fluid dynamics, which collectively regulate primary system pressure and mitigate phase instability. However, many currently operating Nuclear Power Plants (NPPs) face significant long-term operation challenges, largely due to the gradual degradation of systems, structures, and components

over extended service lifetime [3]. This degradation, commonly referred to as "aging", results in changes to material properties and introduces safety concerns that must be carefully addressed and managed [4].

Among the components most susceptible to aging in NPPs is the pressurizer [5]. Aging can significantly affect heat conduction within the pressurizer wall and internal structure, which in term directly influences pressure response time, thermal lag, and structural integrity under normal operation, transient conditions and accident scenarios. Fig. 1 illustrates the pressurizer and its associated primary systems in a standard triple-loop PWR configuration. The U.S. Nuclear Regulatory Commission (NRC) has documented numerous cases in which pressurizers experienced degradation or failures while reactors were operating at power. Notable examples include the Three Mile Island accident (1979), the Calvert Cliffs 2 leakage event (1989), leaks in pressurizer instrument nozzles (1990), cracking in Bugey Unit 3 (1991), cracking events at South Texas and Palo Verde Unit 3 (2003, 2013), pressurizer heater sleeve degradation (2020), pressurizer nozzle weld flaws (2008), and a standby pressurizer heater malfunction at Oconee Station Unit 1 (2024), among others.

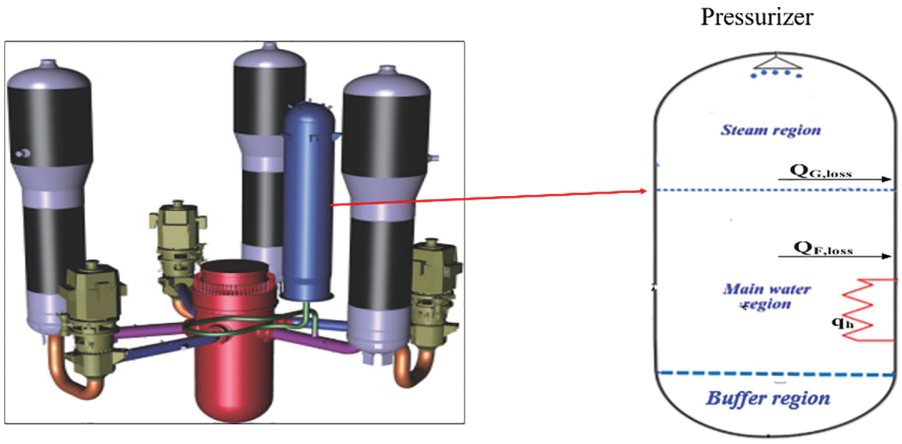

Figure 1: Primary Systems of a triple-loop PWR (left) and the Pressurizer (right).

Accurate and rapid prediction of pressurizer wall temperatures during severe accident scenarios is essential for assessing structural integrity. Such capability can help prevent thermal fatigue and support real-time operational decision-making, and may also inform design improvements and optimization for the next-generation reactor systems. While the T/H literature widely recognizes the importance of modelling thermal effects in reactor components such as pipes and walls, most recent studies have primarily focused on system-level dynamics. Moreover, prior studies indicate that accurately modeling heat conduction in the pressurizer remains challenging due to the high computational cost of detailed calculations [6,7]. This knowledge gap significantly limits the understanding of pressurizer pressure response, thermal lag, and the structural integrity under transient and accident conditions [8].

While system codes such as RELAP5-3D provide high reliable predictions, their substantial computational cost makes them unsuitable for real-time operator support and digital twin integration during rapid evolving transients [9,10]. In such high-stakes environments, the ability to predict thermal gradients within seconds is critical for assessing structural integrity and preventing component failure. To address this limitation, surrogate modeling approaches have been explored, demonstrating significant potential for drastically reducing computational time while retaining acceptable accuracy.

Surrogate models have emerged as a powerful alternative to conventional simulations in NPPs. These models offer computationally efficient calculations, enabling faster analysis and more timely decision-making. For example, Convolution Neural Networks (CNNs) have been successfully applied for nuclear fuel

behavior analysis, significantly reducing simulation time for predicting quantities such as displacement, von Mises stress, and creeping strain [11]. Reduced Oder Models (ROMs) have also demonstrated substantial efficiency gain, decreasing simulation runtimes from days to hours. However, while traditional data-driven models offers significant speed advantages, they may produce results that are numerically accurate yet physically inconsistent, potentially violating fundamental physics principles. For example, Inverse Heat Conduction Problems (IHCPs) have been used in nuclear piping systems to estimate inaccessible internal temperatures and heat fluxes from external measurements [12]. Nevertheless, IHCP-based approaches are well known to be highly sensitive to measurement noise and uncertainties, which can lead to numerical instabilities and non-physical predictions [6]. Collectively, these studies practically highlight the practical need for reliable indirect temperature determination method in high-pressure and high-temperature environments where direct measurements are difficult or infeasible.

To address the black-box nature commonly associated with the Deep Neural Network (DNN), this study bridges this gap by implementing a Physics-Informed Neural Network (PINN) that explicitly embeds the governing heat conduction equation as shown in Eq. (1), which is directly integrated in the neural network loss function.

$$\rho c_p \frac{\partial T}{\partial t} = \nabla \cdot (k \nabla T) \tag{1}$$

This formulation ensures that the surrogate model remains anchored to physical laws, even under extreme transient temperature fluctuations. In this work, we focused on modelling pressurizer temperature profiles during Station Blackout (SBO), Loss-of-Coolant Accident (LOCA) and combined SBO-LOCA scenarios, which represents some of the most challenging and safety-critical accident conditions in NPPs. Prior studies have documented that such transients impose significant thermal and structural challenges on pressurizers [4].

In the present work, a comparative study is conducted among Polynomial Regression, DNN and PINN models. All models are trained and validated using RELAP5-3D data generated from three accident scenarios: SBO, LOCA, and SBO+LOCA conditions. The initial selection of Polynomial Regression as a baseline model was motivated by several factors. It is relative straightforward to understand and implement, and its coefficients can provide limited interpretability regarding the relationship between input variables (time, radial position, boundary temperature) and output variable (temperature). In addition, once trained, Polynomial Regression models offer very fast predictions [13]. A third-order polynomial was selected as it can capture a reasonable level of nonlinearity, making it a suitable baseline for assessing how a simple surrogate model approximates complex thermal behavior before introducing more advanced approaches. However, prior studies have reported that Polynomial Regression models are prone to over fitting –particularly at higher polynomial degree—and may exhibit unreliable extrapolation behavior [14].

The DNN surrogate models were considered as the second modeling approach in this study. DNNs, which are purely Data-Driven (DD) Neural Networks (NN), have been previously applied in PWR safety analysis. For example, Radaideh reported that DNN provided accurate forecasts of peak clad temperature and reactor core pressures during the LOCA scenarios [15]. Despite their strong predictive capability, DNN typically require a large amounts of high-fidelity training data and may struggle to generalize to previously unseen conditions or to consistently enforce physical constraints. For these reasons, the PINN were investigated as the third surrogate modeling approaches in this study, with the aim of improving physical consistency and robustness under transient accident conditions.

The PINN surrogate models directly incorporate the governing heat conduction Partial Differential Equations (PDE) into their loss function during training. This formulation ensures the surrogate models not

only learn from the fed data but are also constrained by the fundamental laws of heat transfer. As a result, PINN promote improved physical consistency and enhanced generalization, particularly in regions with sparse data or under extrapolative conditions. In this study, a PINN model trained on comprehensive temperature profiles spanning from the inner to outer pressurizer wall is expected to exhibit greater robustness and to accurately predict temperatures at arbitrary radial locations for given times and boundary conditions. This work also builds upon our previous research on PINN-based reactor analysis, extending those efforts toward more robust, data-efficient, and physically consistent surrogate modeling frameworks [16].

The training and testing temperature datasets were generated using Reactor Excursion and Leak Analysis Program (RELAP), a well-established system code for T/H transient analysis in PWRs. The pressurizer inner wall temperature data used for surrogate model training were obtained from a one-dimensional (1D) transient heat conduction calculation solved using Finite Difference Method (FDM). Specifically, a Forward Time Central Space (FTCS) methods was employed. This multi-fidelity modeling approach ensures that the surrogate models are trained on physically realistic and high-quality data, thereby improving prediction accuracy and robustness.

The remainder of this paper is structured as follows. Section 2 describes the methodology for primary data generation and the formulation and numerical solution of the transient heat conduction problem using FDM. It also presents the mathematical formulations and training strategies employed for the surrogate models. Section 3 provides a comprehensive validation and comparative performance analysis of the surrogate model, including quantitative evaluation metrics and qualitative visualizations. Finally, Section 4 summarizes the key findings, discusses the implications of the results, and offers recommendations for future research.

2 Methodology

This work uses a multi-step methodology to develop, train, and validate Polynomial Regression, DNN and PINN surrogate models for predicting time-dependent heat conduction in pressurizer wall. The first step was to run three accident cases (SBO, LOCA and SBO+LOCA) with RELAP5-3D. This generated the inner and outer temperatures of the pressurizer wall faces. Second step involved constructing temperature profiles within the pressurizer wall (thickness). Third step focused on constructing, training and testing of the surrogate models. Comprehensive comparative analysis of the surrogate model performances was performed in the last step.

2.1 Postulated Accident Scenarios and Data Generation

Three postulated accident scenarios are selected as case studies as well as for the data generation. SBO represents a complete loss of all Alternating Current (AC) electrical power in the NPPs. This leads to the unavailability of major active safety systems, except for battery supplied components. It is regarded as one of the classical high-pressure accident scenarios, that challenges the NPPs ability to remove decay heat passively [17]. Fukushima Daiichi nuclear accident set as a typical example of a SBO, where all the power to safely operate the reactor went off. On the other hand, LOCA involves a breach in the primary coolant boundary. This results into a rapid drop in reactor system pressure, a decrease in water level as the coolant gushes out through the break. As the coolant is released into the containment, it might lead to a rise temperature and pressure in the pressurizer shell. It is one of the common reported accidents in NPPs, especially, small break loss of coolants (SB-LOCA) [18]. A combined scenario of SBO and LOCA represents a highly severe and challenging transient, integrating the complexities of both a complete loss of AC power and a primary coolant breach in the reactor [19].

The time-dependent inner and outer surface temperature boundary conditions for the pressurizer wall, were obtained from T/H simulations using RELAP5-3D code. RELAP5-3D is a widely recognized and validated high level system code, used in nuclear accident analysis to simulate the overall T/H behavior of reactor systems during accidents, transients and normal states in PWRs [20,21]. The use of RELAP5-3D ensured that the boundary conditions driving the heat conduction in the pressurizer wall, are physically realistic and a good representative of actual PWR during SBO and LOCA scenarios. This approach provides physics based synthetic data, which is crucial for safety analysis, as it ensures high fidelity [22].

2.2 Transient Heat Conduction Problem in Pressurizer

The pressurizer wall consists of two layers, internal cladding (composed of austenitic stainless steel (type 308L)) and main wall (comprised of low-alloy tough carbon steel (type A 516 Mn-Mo steel)). The thermal properties for pressurizer wall (assumed constant) are shown in Table 1. Fig. 2 shows a reconstructed cross section view of the Pressurizer (not drawn to scale).

Table 1: Thermal properties of materials [23].

Property	Type A 516 Mn-Mo Steel (main wall)	Type 308L Stainless Steel (Clad)	Unit
Density ($\boldsymbol{\rho}$)	7850	8000	Kg/m^3
Specific Heat ($\boldsymbol{c_p}$)	500	500	J/Kg·K
Thermal Conductivity ($\boldsymbol{k}$)	33.3	16.2	W/m·K

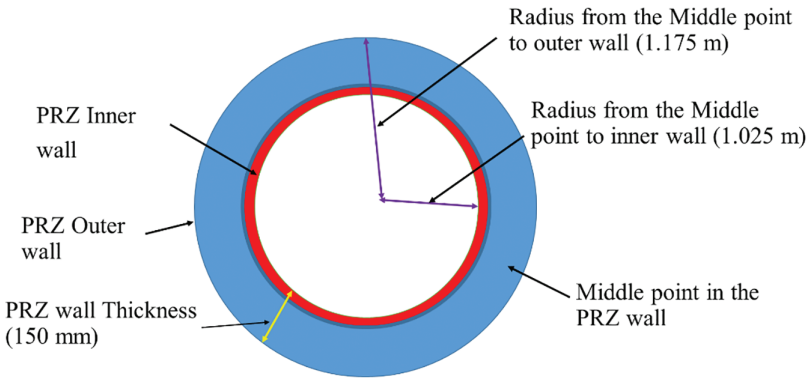

Figure 2: Reconstructed cross-section view of the Pressurizer.

In RELAP simulations, the inner boundary temperature was determined by primary coolant T/H, while the outer boundary temperature resulted from transient conduction through the pressurizer wall. These time dependent wall temperature histories were extracted from RELAP5-3D and applied as Dirichlet boundary conditions in the finite difference and surrogate models.

2.2.1 Mathematical Model

The temperature distribution $T(r,t)$ across the thickness of the pressurizer wall is governed by the 1D transient heat conduction equation in cylindrical coordinates. The general form of this equation is

$$\rho c_p \frac{\partial T}{\partial t} = \frac{1}{r}\frac{\partial}{\partial r}\left(k(r)\, r \frac{\partial T}{\partial r}\right), r \in [r_{in}, r_{out}]\, t > 0 \tag{2}$$

where $T(r,t)$ is the temperature as a function of radius r and time t. $k(r)$ is a piecewise constant function representing the thermal-conductivity of stainless-steel cladding and the carbon-steel base metal. The PINN is designed to minimize the residual of this equation, denoted as $f(r,t)$. The system is subject to the following conditions derived from the RELAP5-3D transient data:

(1) Initial condition

$$T(r,0) = T_{steady}(r)$$

(2) Inner wall boundary condition (fluid-side)

$$-k \left.\frac{\partial T}{\partial r}\right|_{r=r_{in}} = h_{in}(t)\left[T(r_{in},t) - T_{fluid}(t)\right]$$

(3) Outer wall boundary condition (containment-side)

$$\left.\frac{\partial T}{\partial r}\right|_{r=r_{out}} = 0''$$

2.2.2 Numerical Solution Based on Finite Different Method (FDM)

The 1D transient heat conduction equation was solved using Forward Time Central Space (FTCS) explicit finite difference scheme. The wall thickness was spatially discretized into number of radial nodes (Δr). The time domain was discretized into small time steps (Δt). The FTCS scheme was formulated for interior node i at radial position r_i. At the interface between the two materials, heat flux conservation was applied using a harmonic mean for thermal conductivity to ensure accuracy across the boundary.

2.2.3 Wall Temperature Profile Generation and Data Extraction

The FDM model was run for each of the three defined accident cases (SBO, LOCA, SBO+LOCA). For each case, the calculations generated a compressive transient temperature profile $T(r,t)$ across the entire wall thickness (1.025–1.175 m) over the specified accident duration. The spatial discretization employed 100 radial nodes across the wall thickness, with a time step of 1 s. The generated time-dependent temperature profiles (middle and intermediate radial positions) along with the corresponding time and radial position temperature data, was organized into a structured format suitable for training of surrogate models.

2.3 Sampling Techniques

Advanced Design of Experiments (DoE) technique was used to ensure a comprehensive and efficient dataset for surrogate model training. DoE plays a critical role in economically constructing surrogate models with a minimum number of numerical simulations. Latin Hypercube Sampling (LHS) was used to generate a well distributed set of input parameters. This technique divides each input variable's range into equally probable intervals, sampling one value from each interval. It helps to ensure a comprehensive coverage of the multidimensional input space. The stratified sampling approach is good for capturing nonlinear

relationships, and enhancing efficiency in high dimensional spaces. Lastly, Sobol sampling was used as it offers a more evenly distributed sample set than independent and identically distributed uniform samples. This systematic approach ensures that even with a finite number of simulations, the surrogate models are exposed to the most critical thermal gradients and boundary condition variations, minimizing data gaps in the training process.

2.4 Surrogate Models

2.4.1 Polynomial Regression Surrogate Model

A Polynomial Regression surrogate model of a third-order degree was constructed based on a general form shown in Eq. (3). The model was designed to establish a baseline for comparison, allowing a clear assessment of the benefit of more, physic-informed approaches. The model was implemented using a standard least-squares approach. The input features (time and boundary temperatures) were standardized to a zero mean and unit variance to improve numerical stability. The general form of the Polynomial Regression model was

$$T\left(t, r, T_{inner}(\mathrm{t}) \text{ and } T_{outer}(\mathrm{t})\right) = \sum_{i=0}^{N_t}\sum_{j=0}^{N_r}\sum_{k=0}^{N_{in}}\sum_{l=0}^{N_{out}} \beta_{ijkl} t^i r^j \left[\left(T_{inner}(\mathrm{t})\right)^k \left(T_{outer}(\mathrm{t})\right)^l\right] \tag{3}$$

where T is the predicted temperature, t is the time, r is the radial position, $T_{inner}(\mathrm{t})$ and $T_{outer}(\mathrm{t})$ are the time dependent boundary temperatures, β_{ijkl} are the coefficients, and $N_t, N_r, N_{in}, N_{out}$ are the maximum polynomial degrees for each input variable.

2.4.2 DNN Surrogate Model

A supervised DNN was developed to serve as a purely data-driven surrogate model. The DNN consisted of multiple fully connected (dense) hidden layers with a Rectified Linear Unit (ReLU) activation function for nonlinearity. The feedforward DNN architecture of $\hat{T} = \mathcal{N}(r, t; \theta)$, where θ represents the optimized weights and biases. This was implemented using TensorFlow/Kares. The input features consisted of: time elapsed during the accident scenario, radial position within the pressurizer wall, and temperature at both inner and outer surface of the pressurizer (boundary conditions). The output layer consisted of a single neuron with a linear activation function, corresponding to predicted temperature (T_{pred}). The model's performance was optimized by minimizing the MSE loss function as shown in Eq. (4)

$$L_{MSE} = \frac{1}{N}\sum_{i=1}^{N}\left(\left(\dot{T}_{pred,i} - T_{RELAP,i}\right)^2\right) \tag{4}$$

where $\dot{T}_{pred,i}$ is the predicted wall temperature for the data point, and $T_{RELAP,i}$ is the corresponding value yielded from the RELAP and FDM simulations. Adam optimizer was used to minimize the loss, with Mean Absolute Error (MAE), Maximum Absolute Error (MaxAE) and Normalized MAE (NMAE) also monitored as additional evaluation metrics.

2.4.3 PINN Surrogate Model

The PINN incorporated this physical law into its training through a physical loss term ($\mathcal{L}_{phys}$) which is derived from the residual of the governing equation. The PINN model's NN predicts the temperature, $\hat{T}(t, r)$. Its partial derivatives with respect to time and radial position were computed using automatic differentiation,

a feature of the Tensor Flow framework. The PINN minimises a loss function that includes the physics residual $\mathcal{R}(r,t)$ as shown in Eq. (5)

$$\mathcal{R}(r,t) = \rho c_p \frac{\partial \hat{T}}{\partial t} - \frac{1}{r}\frac{\partial}{\partial r}\left(kr\frac{\partial \hat{T}}{\partial r}\right) \tag{5}$$

The optimization objective is defined as the weighted sum of squares as shown in Eq. (6)

$$\min \mathcal{L}(0) = \lambda_{data} MSE_{data} + \lambda_{phys} MSE_{\mathcal{R}} + \lambda_{bc} MSE_{bc} \tag{6}$$

To train the PINN, the physical laws and data constraints are unified into a single composite loss function. The total loss, $\mathcal{L}_{Total}$, is minimized using Adam optimizer and is defined by Eq. (7)

$$\mathcal{L}_{Total} = w_{data}\mathcal{L}_{data} + w_{Phys}\mathcal{L}_{phys} + w_{bc}\mathcal{L}_{bc} + w_{ic}\mathcal{L}_{ic} \tag{7}$$

where $\mathcal{L}_{data}$ is the mean squared error between the PINN's predictions and the RELAP5-3D and FDM-generated temperature data sets. $\mathcal{L}_{phys}$ is the mean square error of the PDE residual, $\mathcal{R}(r,t)$, evaluated at thousands of collocation points throughout the wall thickness. $\mathcal{L}_{bc}$ and $\mathcal{L}_{ic}$are the errors at the boundary (cladding/outer wall) and the initial time step ($t = 0$). w_i are the weighting coefficients (hyper-parameters) that balance the contribution of physics against the data. In this work, all physics-based weights were equal to 1, to prevent one term form dominating training. To ensure robust training and prevent vanishing gradients, all input features (r,t) and targets (T) were scaled to the range $[0,1]$ using min-Max Scaling. Xavier (Glorot) initialization was used to maintain variance across layers. 5000 collocation points were sampled using a Latin Hypercube to ensure the physics loss was evaluated uniformly across the (r,t) domain. Table 2 shows a detailed hyper-parameter for the surrogate models for DNN and PINN architectures.

Table 2: Hyper-parameter setting for the DNN and PINN surrogate models.

Hyperparameter	DNN	PINN
Number of hidden layers	4	4
Neurons per hidden layer	64	64
Activation function	ReLu	Tanh
Optimizer	Adam	Adam
Learning rate	1.0×10^{-3}	5.0×10^{-4}
Number of training epoches	200	200
Loss function	MSE	MSE + PDE residual
Data split (Training/Validation/Test)	90%/5%/5%	90%/5%/5%

2.5 Surrogate Model Validation and Evaluation

To ensure validation, the dataset was split into training, validation and testing subsets. The validation wet was used for early stopping to prevent overfitting. The testing set data was used for final performance reporting. This ensures that the reported metrics reflect the model's true predictive capability on unseen data. Both quantitative and qualitative metrics were used for validation. Standard statistical measures included R-squared (R^2), Root Mean Squared Error (RMSE), MAE, MaxAE and NMAE across training, validation and unseen test datasets. Qualitatively, model performances have been visually assessed through time history

plots, comparing predicted temperatures against simulation and FDM ground truth, at selected radial positions and times. Radial profile plots, illustrating temperature distributions across the wall at specific time snapshots have also been provided.

2.6 Numerical Experiment Setup

To evaluate the accuracy of the surrogate models, we designed three numerical experiments based on T/H transients. In experiment 1 (SBO), we simulated a 10,000 s transient characterised by a total loss of AC power. The experiment 2 (LOCA), represents a sudden depressurization event. This led in rapid fluid temperature fluctuations that impose high thermal gradients on the inner cladding of the pressurizer. Lastly, experiment 3 (SBO + LOCA), is a composite scenario used to generalise across combined worse case accident phenomena. We trained and tested all the models (Polynomial, DNN and PINN) on the three experiments independently. This helps to evaluate the functional consistency of the surrogate models. Table 3 shows a summary of numerical experiment parameters used in the surrogate development.

Table 3: Summary of numerical experiments.

Feature	Specification
Transient duration	10,000 s
Time step Δt	1.0 s
Spatial discretization	100 radial nodes (3 in cladding, 97 in metal)
Input feature	Time inner t, surface temperature T_{in}, outer surface temperature T_{out}
Target output	Radial temperature distribution $T(r,t)$

3 Case Studies and Results

3.1 Data Generation and Case Characteristics

All three accident scenarios commenced from a common initial steady-state condition (at 100 s). During this initial period, the inner pressurizer wall temperature (T_{inner}) was approximately 592 K, with an outer temperature (T_{outer}) of around 318 K. This established a consistent initial temperature gradient across the pressurizer vessel wall. During early reactor transient phase (time 100 to 300 s), a notable thermal drop occurs for all the three scenarios. The T_{inner} remained relatively stable around 560 K. The T_{outer} experienced an increase to approximately 320 K. This rapid equalization of pressurizer surface T_{inner}, suggests an immediate and significant alteration in the external heat transfer conditions. This is likely due to a sudden reduction in external cooling or changes in the primary coolant. Fig. 3 shows the generated RELAP5-3D T_{inner} and T_{outer} profiles for the pressurizer.

3.1.1 SBO Transient Behavior

During the early phase (100–2000 s), T_{inner} dropped from around 690 K to a minimum of around 520 K. Concurrently, T_{outer} dropped from around 590 K to a minimum of around 310 K. This indicates a more gradual cooling effect, as compared to the LOCA cases. During rate phase of the transient (2000 to 10,000 s), both T_{inner} and T_{outer} reached a state of thermal equilibrium at their lower respective temperatures. The absence of a subsequent temperature rise indicates that the system stabilized at a lower energy state following the initial cooling phase.

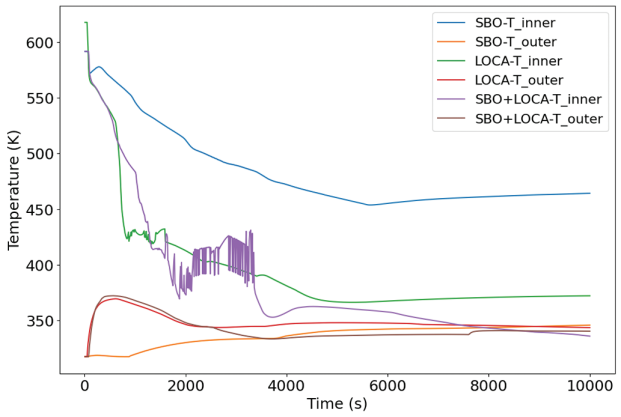

Figure 3: Pressurizer Temperature Profiles during simulated cases.

3.1.2 LOCA Transient Behavior

Like SBO, both T_{inner} and T_{outer} underwent a significant initial decrease during early phase (time 100–3000 s). T_{inner} dropped to minimum of approximately 350 K ~3000–4000 s. T_{outer} also dropped to a minimum ~300 K during the same period. During the later phase of the transient (3000–10,000 s), it was observed that both temperatures stable at these reduced levels. The transient behavior was similar to the SBO case, although the magnitude of the temperature drops were more pronounced for T_{inner}.

3.1.3 SBO+LOCA Transient Behavior

The thermal behavior in the SBO+LOCA case shows an intermediate behavior. Both T_{inner} and T_{outer} showed a similar trend characterized by initial drops, followed by stabilisation at lower temperature levels in the later phases. This suggest that LOCA component might be the dominant factor influencing the thermal response of the pressurizer wall.

3.2 Performance of the Surrogate Models

The adequacy of the training dataset was evaluated through two primary indicators, namely, convergence of the validation loss, and the generalization error on the unseen test set. Qualitative analysis performance time of history, and radial profile plots is provided. Throughout this work, the sampled temperature against time, were at selected radial positions; r = 1.025 m (a) , r = 1.1 m (b), r = 1.12 m (c), and r = 1.175 m (d), as shown in Fig. 4. Location a and d were the inner wall and outer walls of the pressurizer, respectively, while b and c are the intermediate points within the wall. In all the temperature profile plots, "_0" and "_1" represent the true value and model prediction value, respectively. And lastly, temperature profiles across the pressurizer wall at selected time snapshots, which are, T = 2000 s (e), T = 5000 s (f) and T = 8900 s (g) have been provided.

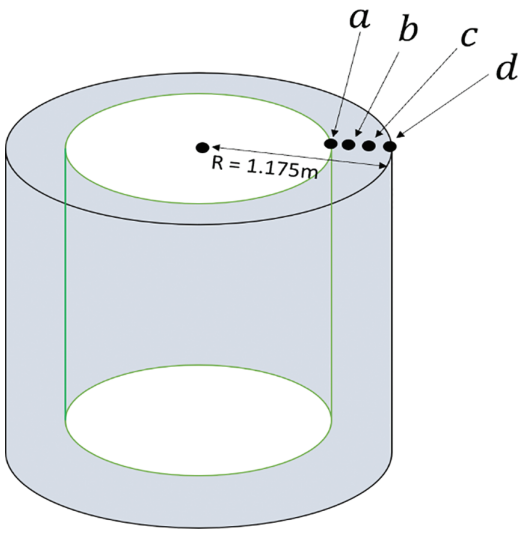

Figure 4: Sampled plotting locations.

3.2.1 Polynomial Regression Model Performance

The model's ability to predict the temperature at any radial position as a function of time was evaluated on unseen data. The model achieved a high coefficient of determination (R^2 = 0.978), indicating that it captures a significant portion of the variance. The consistent performance across training, validation and test set, suggest that the model is not significantly overfitting. The RMSE and MAE are relatively low, indicating a good average fit, as shown in Fig. 5. However, the MaxAE values ranged up to ~200.45 K. This suggests that there were specific instances where its prediction deviates highly from the actual data. The residual distribution plots show non-normal distribution with significant errors, as shown in Fig. 6. The predicted against actual plots (as shown in Fig. 7) show some deviations from the ideal 45-degree line. This confirms the model's low-level ability to accurately capture the nonlinear thermal behavior of the pressurizer wall, making it less reliable for safety-critical analysis.

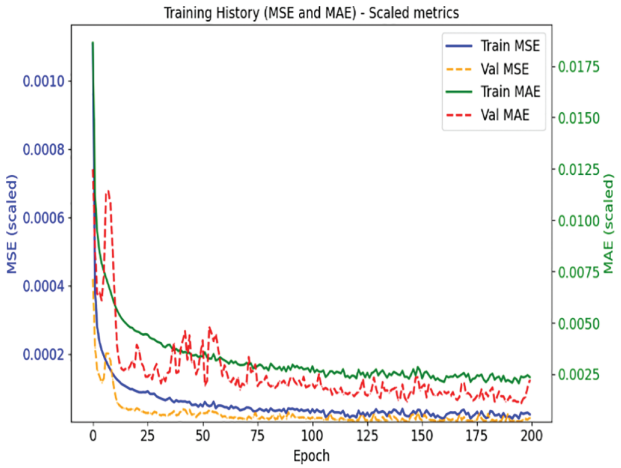

Figure 5: Training and validation losses.

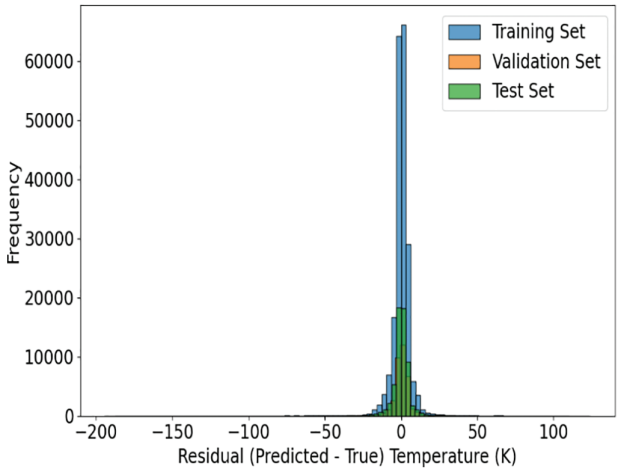

Figure 6: Training set: residual distribution.

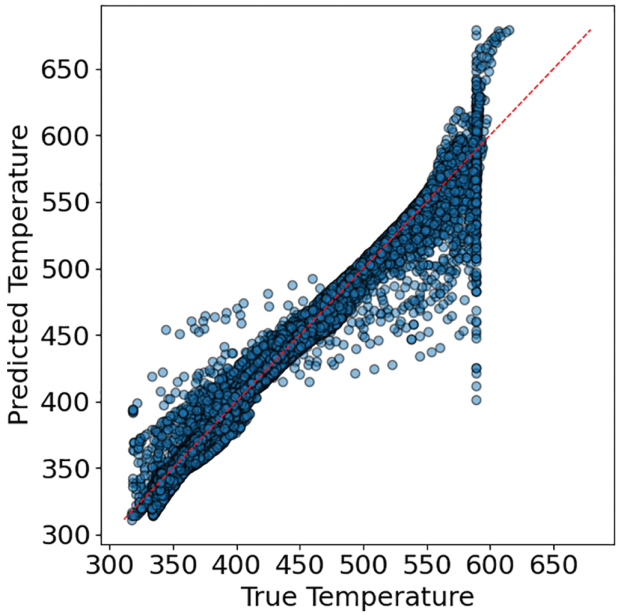

Figure 7: Training set: predicted vs. actual.

The results indicate that the polynomial model's predicted temperature (dashed lines), followed the overall true temperature trend (solid lines) as shown in Fig. 8. However, a few deviations are observed, particularly during phases of rapid temperature changes. For LOCA and SBO+LOCA cases, the model tends to smooth out sharp drops and subsequent fluctuations. The model was more stable for SBO case with its predictions for the middle and outer wall temperatures showing considerable divergence, particularly during the initial transient and later phases.

For LOCA, the model provides a good fit for the radial profiles (Fig. 9). However, SBO+LOCA and mostly SBO, the model shows more significant deviations in the radial profiles, particularly at the inner and outer radial extremes and during the early transient phases (T~2000 s). It was seen that the model tends to smooth out the curvature of the temperature profile across the wall.

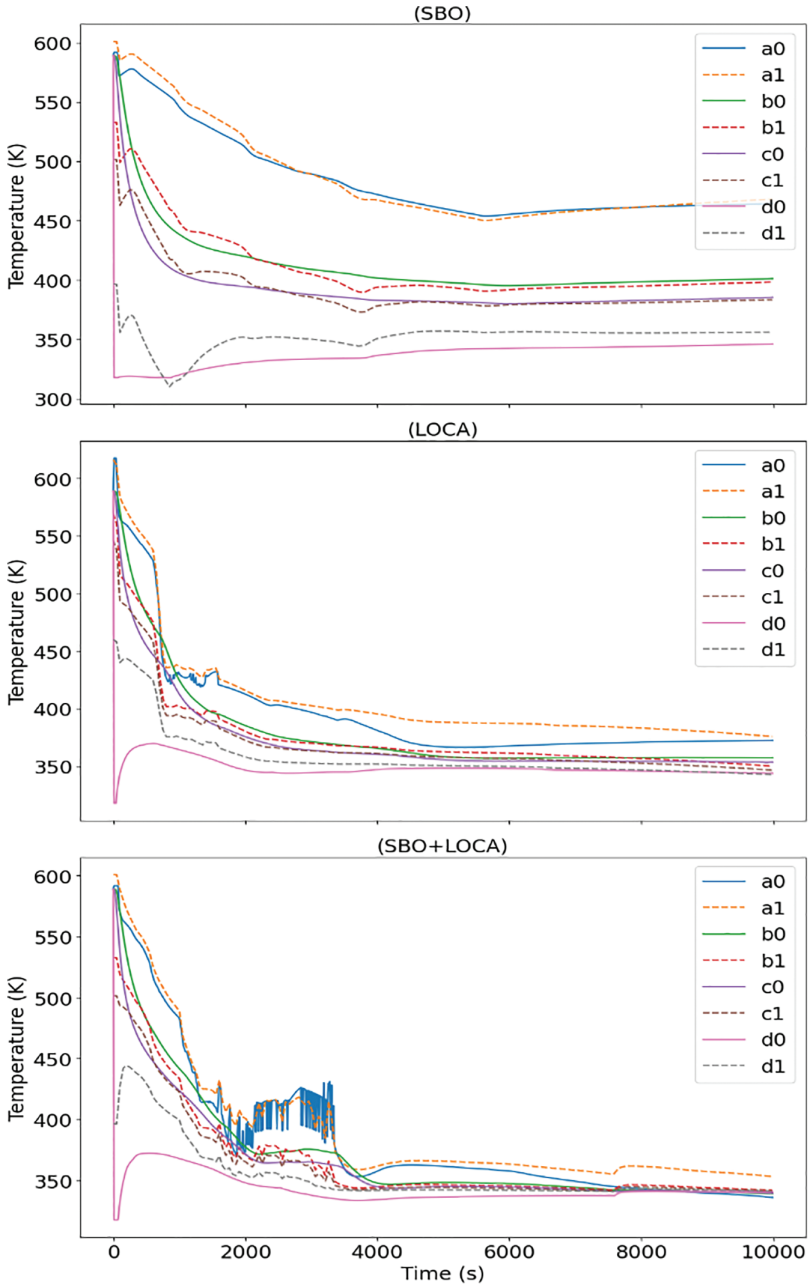

Figure 8: Temperature at selected radii.

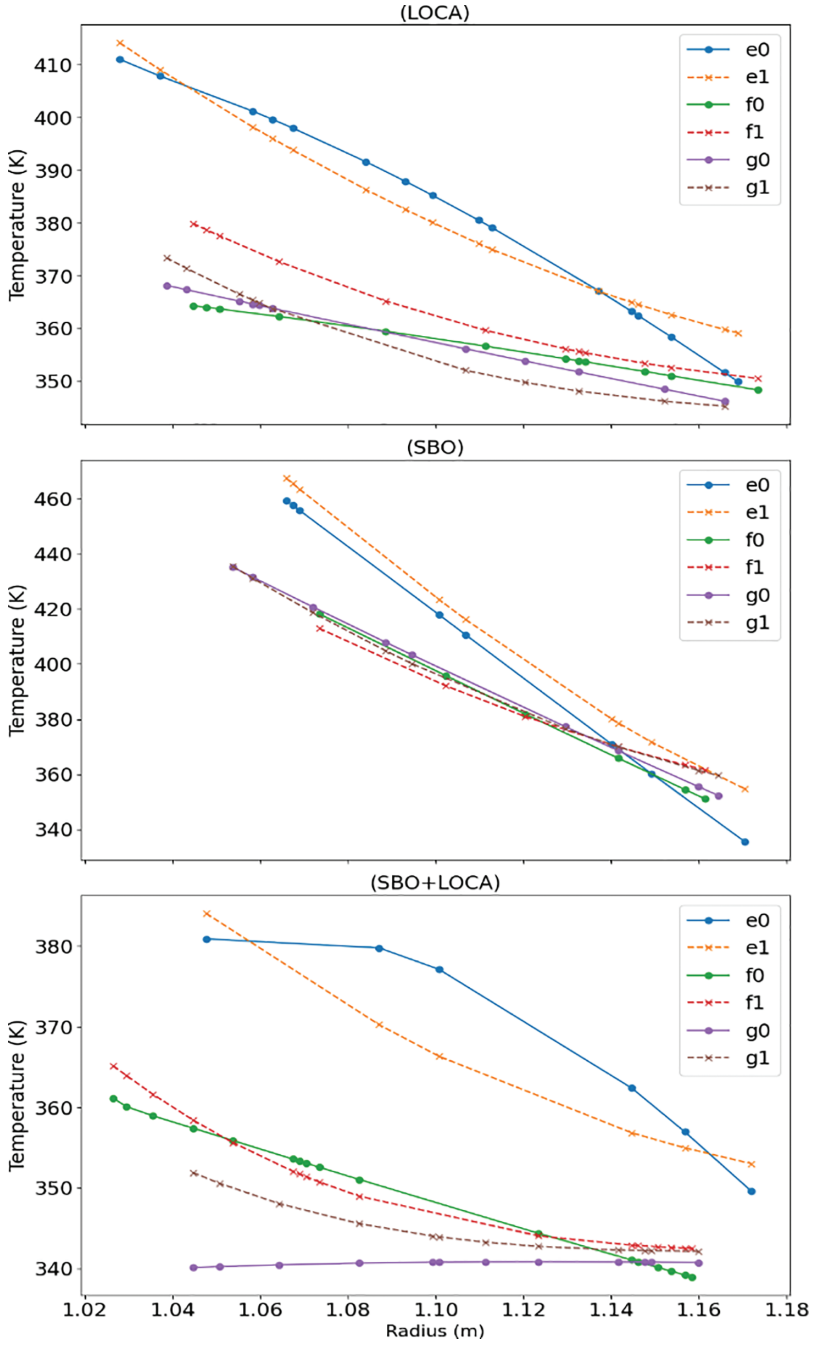

Figure 9: Temperature at selected times.

3.2.2 DNN Model Performance

This model was designed to predict the temperature at any radial position as a function of time. From Table 4, the DNN surrogate model showed exceptionally high performance, achieving an overall $R^2 \approx 0.9996$ on the test set. The overall RMSE ~0.86 K and MAE ~0.52 K represent a significant reduction in average prediction error, as compared to the Polynomial Regression Model. A MaxAE of 44.4 K with NMAE ~0.13 are substantially low (as compared to Polynomial model) suggesting that the DNN model is more robust

in handling extreme temperature deviations. Training and validation loss curves converged rapidly, and the model performance metrics confirms model's high accuracy as shown in Fig. 10. Residual distribution plots, show a symmetric bell-shaped tightly clustered. This indicates model's errors were small and random, as shown in Fig. 11. Fig. 12 shows data points laying on the ideal 45-degree line, indicating that the model provided accurate temperature predictions.

Table 4: Performance metric for the surrogate models.

Surrogate Model	Dataset/case	R^2	RMSE (K)	MAE (K)	MaxAE (K)	NMAE (%)
Polynomial Regression	Training	0.9767	7.69	3.74	200.72	0.97
	Verification	0.9763	7.77	3.76	172.95	0.98
	Test (Overall)	0.9780	7.50	3.74	193.63	0.97
	Test-SBO	0.9765	7.67	3.75	200.45	0.92
	Test-LOCA	0.9767	7.78	3.75	185.2	0.96
	Test-SBO+LOCA	0.9783	7.50	3.74	197.8	0.94
DNN	Training	0.9999	1.06	0.81	18.5	0.17
	Verification	0.9999	0.90	0.62	15.8	0.12
	Test (Overall)	0.9996	1.04	0.79	24.8	0.21
	Test-SBO	0.9998	0.69	0.53	13.72	0.13
	Test-LOCA	0.9996	0.80	0.43	17.78	0.11
	Test-SBO+LOCA	0.9995	1.06	0.60	44.40	0.16
PINN	Training	0.9954	6.76	2.64	58.5	0.66
	Verification	0.9962	6.26	2.77	72.7	0.64
	Test (Overall)	0.9874	5.66	2.63	89.7	0.68
	Test-SBO	0.9848	6.23	2.51	73.67	0.61
	Test-LOCA	0.9853	5.14	2.53	147.92	0.67
	Test-SBO+LOCA	0.9864	5.57	2.87	189.7	0.78

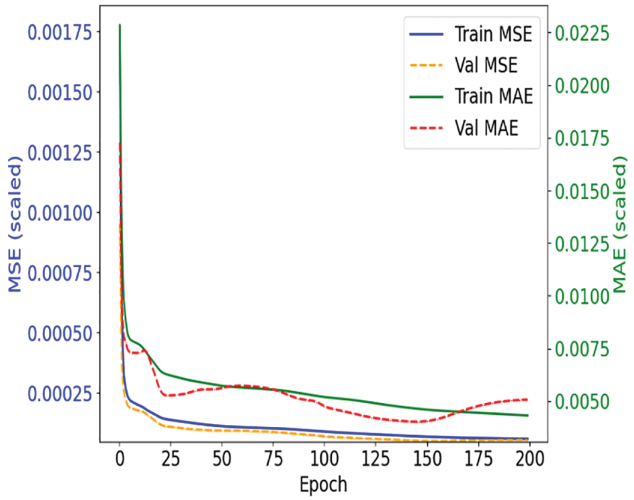

Figure 10: Training and validation losses.

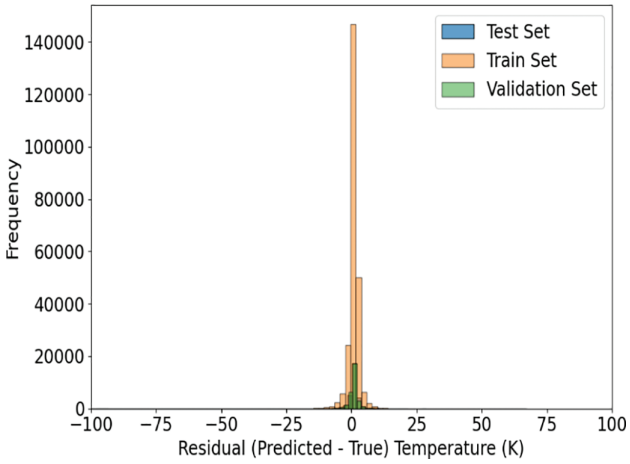

Figure 11: Training set: residual distribution.

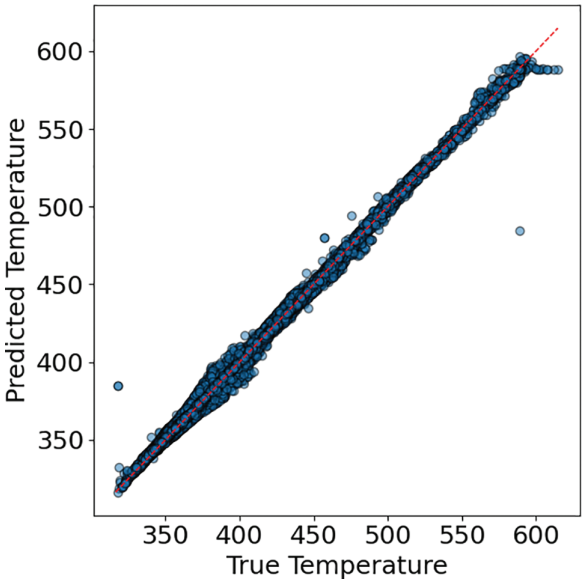

Figure 12: Training set: predicted vs. actual.

The time history plots for the DNN model show a close agreement with the primary data, across the three accident cases. The model captures initial temperature fluctuations, prolonged plateaus and cooling, and re-stabilization trends. For example, (as shown in Fig. 13) in the LOCA and SBO+LOCA scenarios, the DNN model follows the rapid temperature drops and subsequent complex fluctuations with a few minimal deviations. Even in the challenging SBO case, where the polynomial model struggled, the DNN's predictions are better aligned with the primary data, capturing the initial transient and later stabilization phases with high fidelity. Fig. 14 shows that the DNN model, near perfectly alignment with the primary data at selected times across the pressurizer wall radius. This indicates the DNN's robust capability to predict the spatial temperature distribution at any given time, capturing the precise temperature gradients across the pressurizer wall thickness. However, challenges were observed in predicting sharp transients and oscillating temperature trends.

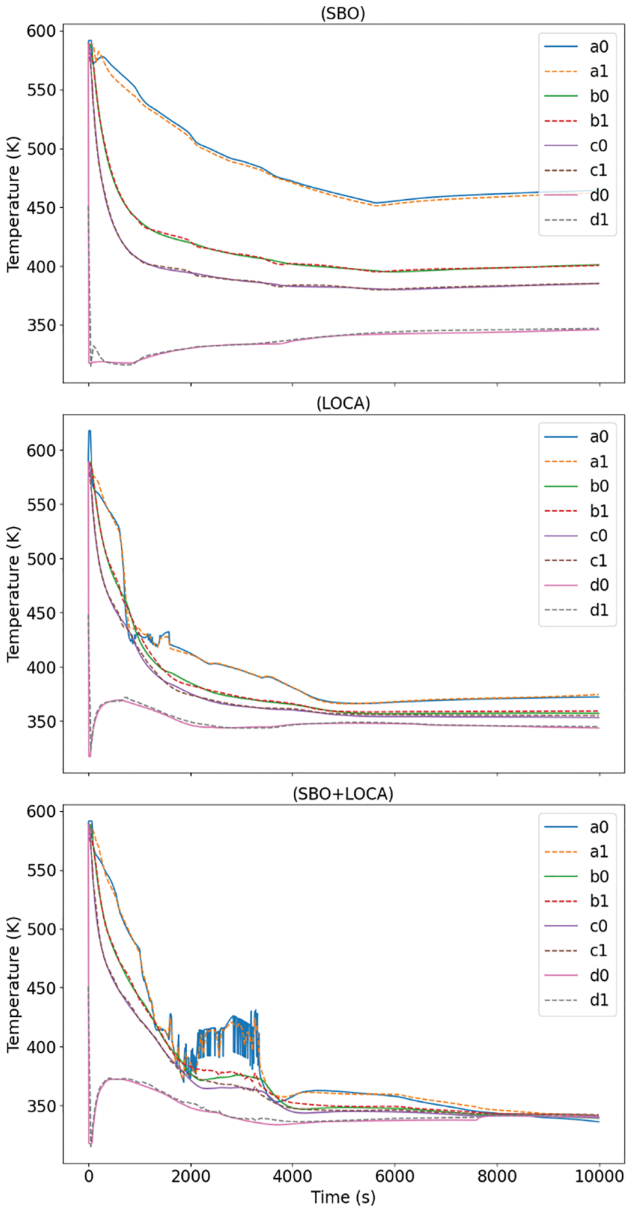

Figure 13: Temperature at selected radii.

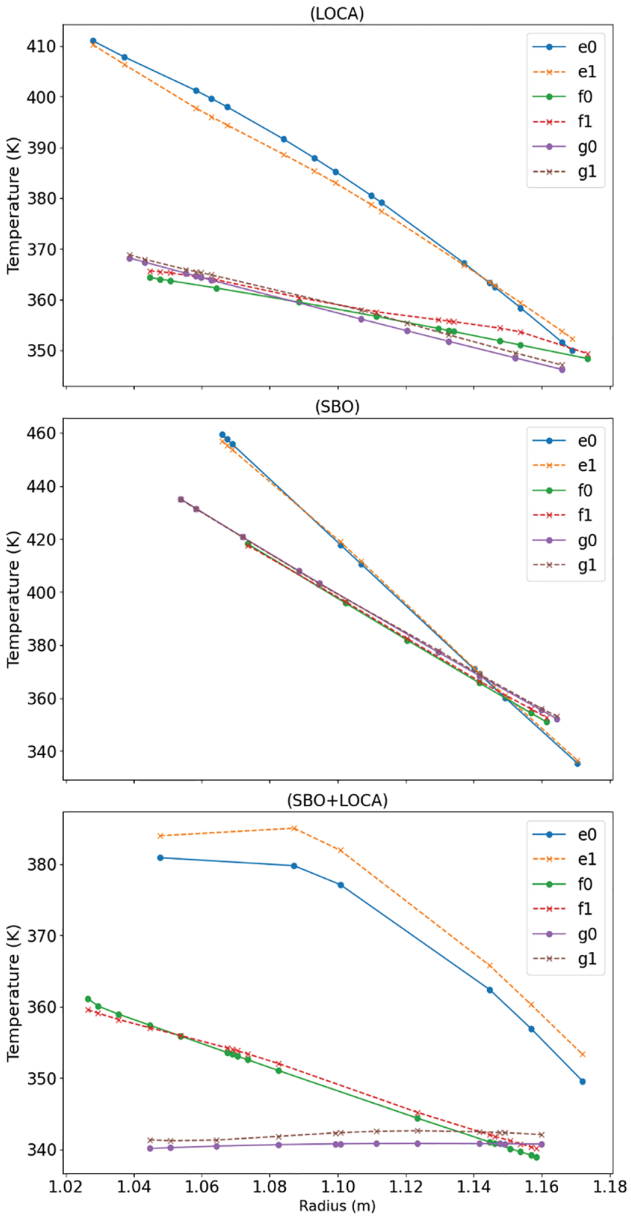

Figure 14: Temperature at selected times.

3.2.3 PINN Model Performance

The PINN model provides a compelling trade-off between statistical accuracy and physical fidelity. While its overall test R^2~0.9874 is lower than that of DNN, its performance is physically consistent. The overall test RMSE ~5.66 K and MAE ~2.63 K are better than the polynomial regression model. As seen in Fig. 15 (Training and Validation Loss), the model's loss curves show a steady and consistent decrease. This indicates that the network effectively learned for both the primary temperature data and the physics constraints without overfitting. The performance metrics in Table 4 confirms this, with a higher R^2 and moderate error values seen across the training, validation and test sets.

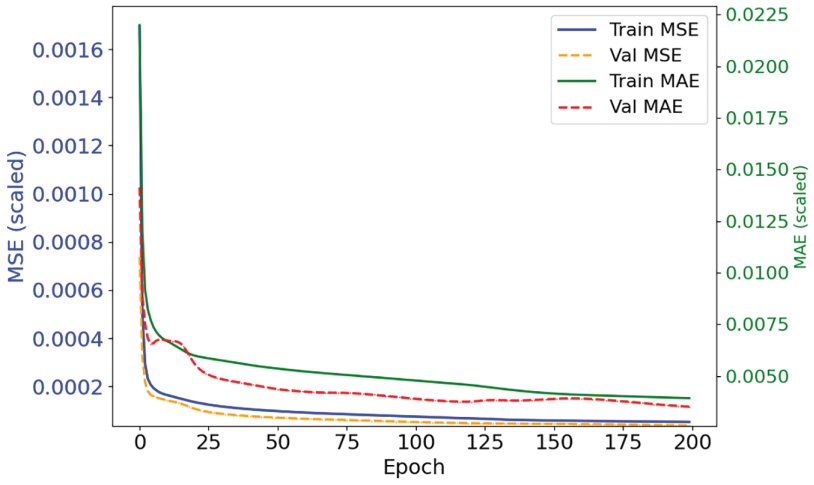

Figure 15: Training and validation losses.

The residual distribution plots (Fig. 16) indicates less clustered, as compared to purely data-driven models, with small and random distributed errors. However, this is still well centered around zero. The predicted against the actual plots (Fig. 17) show that data points closely align with the ideal 45-degree line. This suggest that incorporating physical constraints is highly effective at capturing the dynamics of multi-regime transients, providing a more reliable tool for safety analysis.

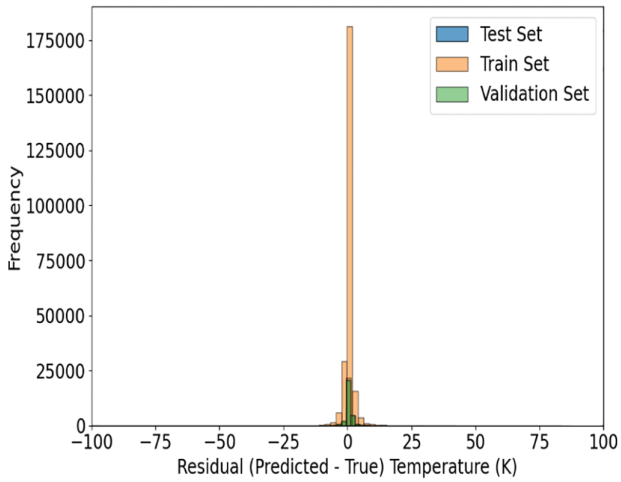

Figure 16: Training set: residual distribution.

The PINN predicted plots for selected radial position (Fig. 18), indicate that the model effectively captures the temperature trends at different depths within the pressurizer wall. The close agreement between the PINN and primary data, indicates that the model accurately learns and simulates the transient thermal behavior over time. Surprisingly, this included the rapid changes during the early phase of a transient and the slower progression to steady state. Lastly, Fig. 19 shows point wise validation of the PINN model's performance, indicating its reliability and accuracy. Therefore, the use of PINN in pipes such as pressurizer, could be pivotal in understanding the thermal transient behavior, as a substitute of IHPC.

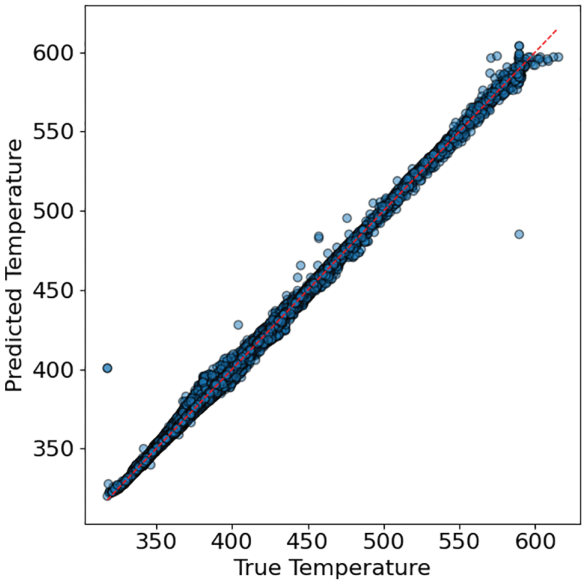

Figure 17: Training set: predicted vs. actual.

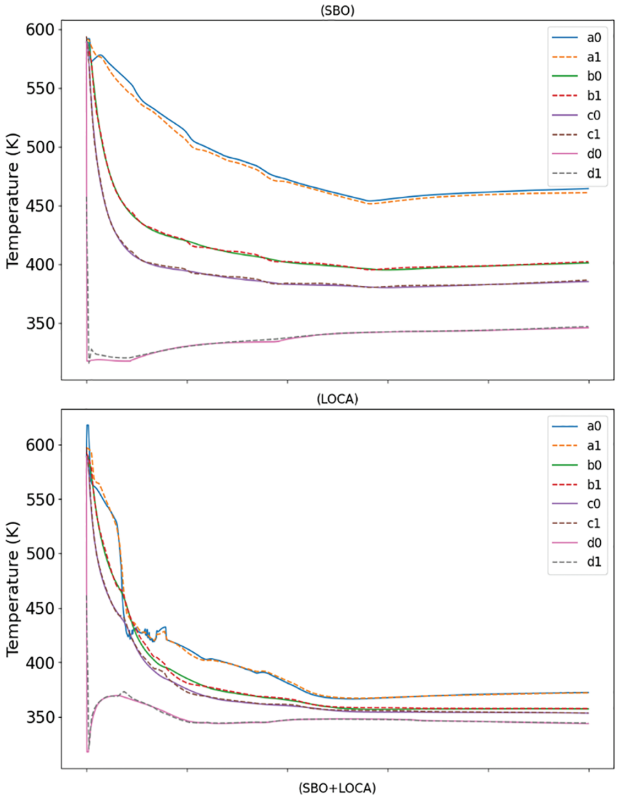

Figure 18: (Continued)

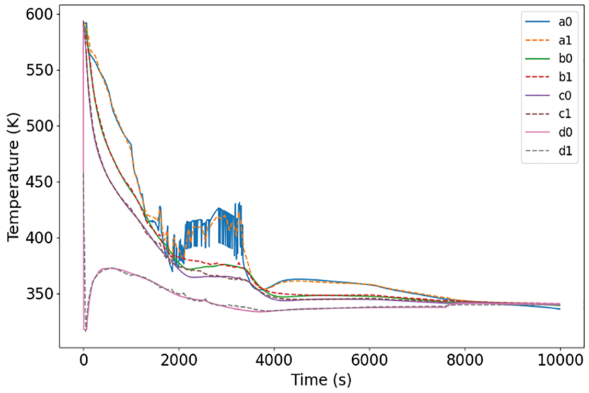

Figure 18: Temperature at selected radii.

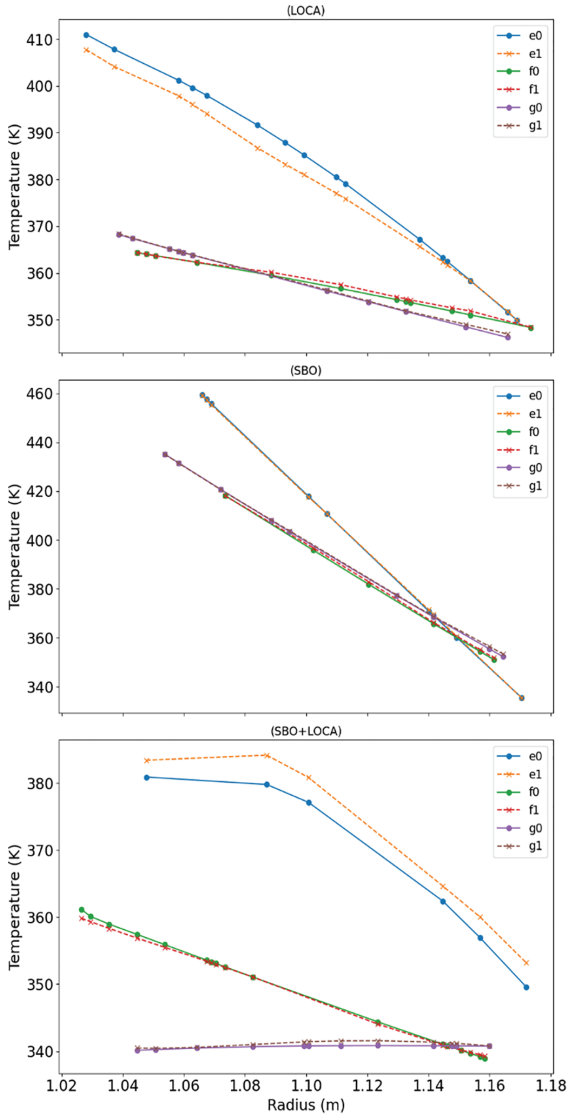

Figure 19: Temperature at selected times.

Although the DNN achieves the lowest numerical errors, it occasionally produces non-physical behavior during sharp transients, such as oscillatory temperature predictions and slight violations of the expected monotonic radial gradient. In contrast, the PINN maintains smooth, physically consistent profiles across the pressurizer wall. This is because its solution its constrained by the heat-conduction PDE. For example, during the early rapid-cooling phase of the LOCA case (t = 1500–2500 s), the DNN model slightly overshoots the mid-wall temperature, whereas the PINN preserves the correct curvature and gradient, dictated by the governing physics. The PINN ensures that the temporal and spatial derivatives are coupled according to the material's thermal diffusivity. This provides a more reliable basis for subsequent thermal stress and structural integrity assessment.

3.3 Comparative Analysis of Surrogate Models

Quantitative performance of each surrogate model across all test cases is show in Table 4. The performance metrics demonstrate that the surrogate models maintain consistent accuracy when evaluated on these independent cases.

Validation and comparative analysis of the Polynomial Regression, DNN and PINN surrogate models, show distinct capabilities in predicting time-depended heat conduction in the pressurizer wall under severe accident cases. The Polynomial Regression model indicate a reasonable general fit. It had a fastest convergence to solutions, as compared to both DNN and PINN surrogate models. However, the model had a MaxAE ~200.45 K, suggesting a need to investigate other better surrogate models. It also struggled to accurate capture sharp thermal transients and complex fluctuations, particularly in the SBO case where its predictions for the middle and outer walls had a few divergences from the simulation data. Overall, the results indicate that the model could led to a significant underestimation or overestimation of thermal stresses. This may compromise the structural integrity assessment of the pressurizer wall.

The DNN model showed a better performance across all the quantitative metrics. The history time plots were all close to the real data sets, capturing intricate temperature changes. Therefore, this model had better capabilities to model non-linear thermal dynamics of the pressurizer wall, under diverse transient conditions. It significantly outperformed the fixed-degree polynomial approach. The main drawback is in capturing high temperature fluctuations and maintaining physical consistency. The PINN provides a compelling trade-off between statistical accuracy and physical fidelity. While its overall physical test R^2~0.9892 is lower than the DNN, its performance is still exceptional and physically consistent. The overall test RMSE~3.55 K and MAE~1.46 are a good improvement over the polynomial model. Qualitative analysis of temperature profiles confirmed the PINN's ability to accurately capture complex non-linear thermal behaviors across all the postulated accident cases.

A key sample of the PINN's advantage is its observed performance in data-sparse regions, and during high gradient transients, like the start of LOCA event. In these scenarios, the DNN's lack of physical constraints can lead to localized non-physical temperature wiggles, if the training data is not sufficiently dense. The PINN acts as a regularized model where the physics loss term penalises such artifacts, ensuring that the predicted cooling rates and internal thermal lags remain the bounds of physical reality. Also, more importantly, the PINN model was able to capture high-frequency temperature oscillations, and eliminates phase lag. This makes PINN a better candidate than DNN for T/H assessment, in scenarios of high temperature fluctuations.

The application of PINN in this study, demonstrates the feasibility of integrating physical laws, with data-driven learning to model transient heat conduction in NPP pipes. The incorporation of governing PDEs, initial and boundary conditions helped to improve generalization in data sparse regions, while reducing reliance on extensive simulation data. The encouragement performance obtained in this work,

highlights the potential of PINN as a complementary tool in safety assessment. This would be of great use, particularly where conventional simulations may computationally be expensive for real-time analysis. However, challenges were observed in optimizing network architecture, balancing loss weights and scaling. This suggests a need for continued training and benchmarking surrogate models against high-fidelity codes, to establish reliability and regulatory acceptance.

4 Conclusion and Recommendation

In this study, both data-driven and physics-informed surrogate models were developed and compared for predicting the transient temperature distribution in a PWR pressurizer wall during severe accident scenarios. Based on the results, the following conclusions are drawn:

(1) All models are capable of providing temperature predictions in near real time (on the order of milliseconds). This represents a significant computational speed-up compared to conventional RELAP5-3D and FDM simulations, which are computationally intensive for online monitoring applications.
(2) While all three models achieved high statistical accuracy, the DNN exhibited the highest numerical precision with R^2 of approximately 0.9996 and the lowest RMSE, making it a an effective interpolator for known temperature datasets.
(3) The PINN achieved a favourable balance between statistical accuracy (R^2 = 0.987) and physical consistency. Unlike the DNN, the PINN enforces satisfaction of the governing heat conduction equation, ensuring the predicted temperature gradients remain physically meaningful, which is critical for trustworthy nuclear safety assessments.
(4) The PINN model was able to capture high-frequency temperature oscillations, and to eliminate non-conservative peak predictions errors and phase lag in regions where data-driven models tend to struggle. This capability makes the PINN a more suitable candidate than the DNN for T/H assessments under conditions involving strong transient oscillations.
(5) The successful application of these models to complex SBO and LOCA transients, demonstrates their potential for integration into digital twin frameworks for NPPs. Such integration could enable rapid structural integrity evaluations and thermal stress assessments during emergency conditions.
(6) This work further confirms that incorporating physics-based loss terms acts as an effective regularization mechanism, reducing the risk of non-physical predictions in data sparse regions when compared to purely data-driven methods.

Future studies will focus on improving the robustness of PINN implementations, including the integration of Uncertainty Quantification (UQ) methods like Bayesian NNs and exploration of advanced data sampling strategies. To transition these models from research tools to practical engineering solutions, validation against experimental or real reactor operational data will be required. Additional extensions may include consideration of more complex scenarios, such as 3D geometries and fully coupled multiphysics phenomena.

Acknowledgement: This work was performed with the support of the U.S Department of Energy's Nuclear Energy University Program (NEUP) with the award No. DE-NE-0009505. This research has made use of the resources of the High-Performance Computing Center at Idaho National Laboratory, which is supported by the Office of the Nuclear Energy of the U.S Department of Energy and the National Science User Facilities under Contract No. DE-AC07-051D1517.

Funding Statement: This work was performed with the support of the U.S Department of Energy's Nuclear Energy University Program (NEUP) with the award No. DE-NE-0009505.

Author Contributions: Fabiano Thulu: conceptualization, methodology, software, investigation, data curation, formal analysis, visualization, writing—original draft. Zeyun Wu: Conceptualization, supervision, funding acquisition, validation, writing—review & editing. All authors reviewed and approved the final version of the manuscript.

Availability of Data and Materials: The datasets and materials generated and/or analysed during the current study are available from the corresponding author upon reasonable request.

Ethics Approval: This study did not involve human participants, human data, or animal subjects, and therefore ethical approval was not required.

Conflicts of Interest: The authors declare no conflicts of interest.

Nomenclature

$\dot{T}_{pred}$	Predicted temperature
h_{in}	Inner heat flux
T_{RELAP}	RELAP Temperature
T_{fluid}	Fluid temperature
T_{steady}	Temperature at steady state
c_p	Specific heat
r_i	Radial node position
r_{in}	Inner radius
r_{out}	Outer radius
Δr	Number of radial nodes
Δt	Time step
∇	Nabla
$a0$	True temp at 1.025 m
$a1$	Predicted temp at 1.025 m
$b0$	True temp at 1.1 m
$b1$	Predicted temp at 1.1 m
$c0$	True temp at 1.12 m
$c1$	Predicted temp at 1.12 m
$d0$	True temp at 1.175 m
∂	Partial differential
$d1$	Predicted temperature at 1.175 m
$e0$	True temperature at 2000 s
$e1$	Predicted temperature at 2000 s
$f0$	True temperature at 5000 s
$f1$	Predicted temperature at 5000 s
$g0$	True temperature at 8900 s
$g1$	Predicted temperature at 8900 s
$\mathcal{L}$	Laplace Transform
$\mathcal{R}$	Riemann integral
T	Kelvin temperature
i	Interior node
k	Thermal conductivity
r	Radius
t	Time
$\mathcal{N}$	Normal distribution
β	Beta
θ	Angle

λ	lambda
ρ	Density
ϵ	Epsilon

Abbreviations

AC	Alternating Current
CNNs	Convolution Neural Networks
DD	Data-Driven
DNN	Deep Neural Network
DoE	Design of Experiments
FDM	Finite Different Method
FTCS	Forward Time Central Space
IHCPs	Inverse Heat Conduction Problems
LHS	Latin Hypercube Sampling
LOCA	Loss of Coolant Accident
MAE	Mean Absolute Error
MaxAE	Maximum Absolute Error
NMAE	Normalized Mean Absolute Error
NN	Neural Networks
NPPs	Nuclear Power Plants
NRC	Nuclear Regulatory Commission
PDE	Partial Differential Equation
PINN	Physics-Informed Neural Network
PWR	Pressurized Water Reactors
ReLU	Rectified Linear Unit
RELAP	Reactor Excursion and Leak Analysis Program
RMSE	Root Mean Squared Error
ROMs	Reduced Oder Models
SBO	Station Blackout
T/H	Thermal-Hydraulics
UQ	Uncertainty Quantification

References

1. Alschuler WR. Nuclear energy and climate change. Phys Today. 2024;77(11):10–1. doi:10.1063/pt.arcp.uytt.
2. Cancemi SA, Lo Frano R. Preliminary study of the effects of ageing on the long-term performance of NPP pipe. Prog Nucl Energy. 2021;131(2):103573. doi:10.1016/j.pnucene.2020.103573.
3. Farman NF, ALasadi S, Ali Abdul Redha Z. A review of advances in pressurizer response research for pressurized water reactor systems. Int J Simul Syst Sci Technol. 2018;19(2):1–11. doi:10.5013/ijssst.a.19.02.03.
4. Katinas C, Reichardt T, D'Entremont B, Ray W, Willis M, Kulp T. Calculation of nuclear reactor cooling tower performance with limited data streams. J Therm Sci Eng Appl. 2023;15(1):011013. doi:10.1115/1.4055746.
5. El-Genk MS, Altamimi R, Schriener TM. Pressurizer dynamic model and emulated programmable logic controllers for nuclear power plants cybersecurity investigations. Ann Nucl Energy. 2021;154:108121. doi:10.1016/j.anucene.2020.108121.
6. Lu T, Han WW, Jiang PX, Zhu YH, Wu J, Liu CL. A two-dimensional inverse heat conduction problem for simultaneous estimation of heat convection coefficient, fluid temperature and wall temperature on the inner wall of a pipeline. Prog Nucl Energy. 2015;81:161–8. doi:10.1016/j.pnucene.2015.01.018.
7. Sikorska D, Brzozowska J, Pawełkiewicz A, Psykała M, Błasiak P, Kolasiński P. Convective heat transfer in PWR, BWR, CANDU, SMR, and MSR nuclear reactors—a review. Energies. 2024;17(15):3652. doi:10.3390/en17153652.
8. Lo Frano R, Cancemi SA, Darnowski P, Ciolini R, Paci S. Preliminary analysis of an aged RPV subjected to station blackout. Energies. 2021;14(15):4394. doi:10.3390/en14154394.

9. Diao X, Zhao Y, Smidts C, Vaddi PK, Li R, Lei H, et al. Dynamic probabilistic risk assessment for electric grid cybersecurity. Reliab Eng Syst Saf. 2024;241(9):109699. doi:10.1016/j.ress.2023.109699.
10. Abio A, Bonada F, Garcia-Llamas E, Grané M, Nievas N, Lange D, et al. A transfer learning method in press hardening surrogate modeling: from simulations to real-world. J Manuf Syst. 2014;77:320–40. doi:10.1016/j.jmsy.2024.09.012.
11. She J, Shi T, Xue S, Zhu Y, Lu S, Sun P, et al. Diagnosis and prediction for loss of coolant accidents in nuclear power plants using deep learning methods. Front Energy Res. 2021;9:665262. doi:10.3389/fenrg.2021.665262.
12. Wahlquist S, Hansel J, Sabharwall P. A critical review of heat pipe experiments in nuclear energy applications. Nucl Sci Eng. 2023;197(5):719–52. doi:10.1080/00295639.2022.2082230.
13. Radaideh MI, Kozlowski T. Surrogate modeling of advanced computer simulations using deep Gaussian processes. Reliab Eng Syst Saf. 2020;195:106731. doi:10.1016/j.ress.2019.106731.
14. Wang K, Li F, Zhou T, Wang D. Kriging surrogate model for optimizing outlet temperature distribution in low-emission combustors without dilution holes. AIP Adv. 2024;14(5):055310. doi:10.1063/5.0198258.
15. Radaideh MI, Pigg C, Kozlowski T, Deng Y, Qu A. Neural-based time series forecasting of loss of coolant accidents in nuclear power plants. Expert Syst Appl. 2020;160:113699. doi:10.1016/j.eswa.2020.113699.
16. Elhareef MH, Wu Z. Physics-informed neural network method and application to nuclear reactor calculations: a pilot study. Nucl Sci Eng. 2023;197(4):601–22. doi:10.1080/00295639.2022.2123211.
17. Thulu FGD, Elshahat A, Hassan M. Safety analysis in VVER-1000 due to large-break loss-of-coolant accident and station blackout transient using RELAP5/SCDAPSIM/MOD3.5. Nucl Sci Eng. 2022;196(5):568–83. doi:10.1080/00295639.2021.2009984.
18. Skolik K, Allison C, Hohorst J, Malicki M, Perez-Ferragut M, Pieńkowski L, et al. Analysis of loss of coolant accident without ECCS and DHRS in an integral pressurized water reactor using RELAP/SCDAPSIM. Prog Nucl Energy. 2021;134:103648. doi:10.1016/j.pnucene.2021.103648.
19. Ali Hosseini S, Shirani AS, Zangian M, Najafi A. Re-assessment of accumulators performance to identify VVER-1000 vulnerabilities against various break sizes of SB-LOCA along with SBO. Prog Nucl Energy. 2020;119:103145. doi:10.1016/j.pnucene.2019.103145.
20. Liu T, Wu Z, Bensi M, Ma Z. A mechanistic model of a PWR-based nuclear power plant in response to external hazard-induced station blackout accidents. Front Energy Res. 2023;11:1191467. doi:10.3389/fenrg.2023.1191467.
21. Thulu FGD, Elshahat A, Hassan MHM. Simulation of VVER-1000 guillotine large break loss of coolant accident using RELAP5/SCDAPSIM/MOD3.5. J Nucl Eng. 2021;2(4):516–32. doi:10.3390/jne2040035.
22. Prošek A, Mavko B. RELAP5/MOD3.3 best estimate analyses for human reliability analysis. Sci Technol Nucl Install. 2010;2010:797193. doi:10.1155/2010/797193.
23. Mohanty S, Soppet WK, Majumdar S, Natesan K. Thermal-mechanical stress analyisis of PWR pressure vessel and nozzle under grid load-following mode. Interim report on the effect of cyclis hardening properties and pre-existing cracks on stress analysis results. Argonne, IL, USA: Argonne National Laboratory; 2016. Report No.: ANL/LWRS-16/01.